Electron paramagnetic resonance studies of silicon-related defects in diamond

A. M. Edmonds and M. E. Newton*
Department of Physics, University of Warwick, Coventry CV4 7AL, United Kingdom

P. M. Martineau
DTC Research Centre, Belmont Road, Maidenhead, Berkshire SL6 6JW, United Kingdom

D. J. Twitchen and S. D. Williams
Element Six Ltd., King's Ride Park, Ascot, Berkshire SL5 8BP, United Kingdom

(Received 7 February 2008; revised manuscript received 5 April 2008; published 11 June 2008)

We report the results of multifrequency electron paramagnetic resonance studies at temperatures between 8 and 300 K on diamonds synthesized by chemical vapor deposition and intentionally silicon doped with isotopes in natural abundance or isotopically enriched. The ^{29}Si hyperfine structure has provided definitive evidence for the involvement of silicon in two electron paramagnetic resonance centers in diamond that were previously suspected to involve silicon: KUL1 and KUL3. We present data that unambiguously identify KUL1 as an $S=1$ neutral silicon split-vacancy (D_{3d} symmetry) defect $(V\text{-Si-}V)^0$, while KUL3 is shown to be $(V\text{-Si-}V)^0$ decorated with a hydrogen atom, $(V\text{-Si-}V\text{:H})^0$.

DOI: 10.1103/PhysRevB.77.245205 PACS number(s): 81.05.Uw, 61.72.jn, 76.30.Mi

I. INTRODUCTION

Advances in single-crystal (SC) diamond synthesis by the chemical vapor deposition (CVD) method have stimulated interest in utilizing this material in a variety of applications wherein its extreme properties can be exploited. Of particular interest is the combination of high electron and hole mobilities[1] (4500 and 3800 $cm^{-2}\,V^{-1}\,s^{-1}$, respectively), breakdown strength[2] (10^7 V cm^{-1}) and thermal conductivity[3] (in excess of 2000 W $m^{-1}\,K^{-1}$), which enable diamond to surpass other wide band gap materials for high power and high frequency electronic applications. However, the electronic properties of diamond are limited by defects and impurities grown into the material and introduced during the processing steps involved with device fabrication. This motivates work on understanding and determining the electronic properties and lattice structures of defects and/or impurities in CVD diamond.

CVD diamond is synthesized in an environment that contains a number of potential sources of silicon, including the walls and/or windows of the reactor, or in the case of heteroepitaxial growth of diamond on silicon, the substrate itself. Etching of these sources[4,5] has been used to explain the common contamination of CVD diamond with silicon, with its presence inferred from the 737 nm system, observed in luminescence and absorption.

A. 737 nm optical center in diamond

A line at 737 nm (1.68 eV) was first observed by Vavilov *et al.*[6] in cathodoluminescence investigations of homoepitaxial diamond layers and polycrystalline films grown on silicon substrates. Subsequent ion implantation experiments determined that this line is also present in natural diamond that has been implanted with silicon ions, suggesting that this element is involved in the formation of this defect.[7] However, the unambiguous association of this center with silicon was not possible until single-crystal high-pressure high-temperature (HPHT) grown diamonds were deliberately doped with silicon, achieved by adding 10% silicon to the graphite in the growth cell.[8] The higher quality and relatively stress-free nature of such samples allowed low-temperature photoluminescence (PL) and absorption experiments to resolve the 12-lined fine structure of the 737 nm center.[9] It was found to be comprised of three groups of four lines, with the intensity of each group scaling with the natural abundances of the isotopes of silicon. The four component lines for each isotope were associated with a transition from an orbitally degenerate ground state, split by 0.2 meV, to a doublet excited state split by 1.07 meV.[9]

In studies of the 737 nm center, it has also been shown that electron irradiation and subsequent annealing above 700 °C leads to an increase in the emission and absorption intensity, with the defect surviving annealing temperatures in excess of 2000 °C.[10,11] Since 700 °C is the temperature at which the vacancy in diamond becomes mobile,[12] these findings suggest that the 737 nm optical center involves both silicon and vacancies. The increase in intensity upon annealing also requires that silicon is present in other forms in as-grown material and that it acts as an effective trap for mobile vacancies.

In order to reconcile the involvement of silicon and vacancies in the 737 nm defect, theoretical work, using local density functional theory, has been undertaken on substitutional silicon adjacent to a vacancy, (Si_s-V). Goss *et al.*[13] suggested that the silicon atom is unstable at a substitutional site and that the system relaxes to a split-vacancy structure that has D_{3d} symmetry (see Fig. 1). In this paper, we will refer to this structure as (V-Si-V). Such a split-vacancy structure was found for the tin-vacancy center in silicon;[14] tin (silicon) is a large isoelectronic impurity in silicon (diamond).

For $(V\text{-Si-}V)^0$, it is predicted that the ground state is $^3A_{2g}$; but since this is orbitally nondegenerate, this cannot account for the observed 737 nm system. However, calculations suggest that (V-Si-V) has an acceptor level at around E_v +1.5 eV.[15,16] $(V\text{-Si-}V)^-$ is predicted to have a ^2E_g ground

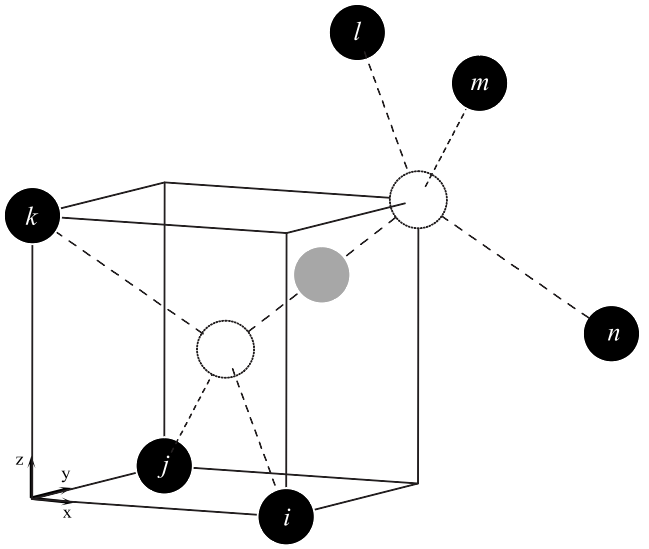

FIG. 1. The structure of the silicon split-vacancy center (*V*-Si-*V*). The solid black circles (labeled *i*-*n*) represent carbon atoms, the lighter circle indicate the relaxed silicon site, and the white circles indicate the vacancies.

state and a $^2E_g \rightarrow {}^2E_u$ optical transition at ~1.9 eV, in tolerable agreement with the 1.68 eV observed. The suggestion that the 1.68 eV center is a negatively charged defect is supported by the experiments of Collins *et al.*,[17] who detected the defect only in samples containing substitutional nitrogen (N_s), which could act as a donor.

Polarized PL,[18] uniaxial stress,[19] and Zeeman splitting[19] measurements on the 737 nm system have suggested that the defect responsible has a tetragonal or lower symmetry. Both the positive and the negative charge states of (*V*-Si-*V*) are subject to a Jahn–Teller distortion, which lowers the symmetry.[20] Hence, the 737 nm system may indeed originate from $(V\text{-Si-}V)^-$, but further experimental and theoretical work is required to confirm this association. In addition, no other silicon-related defects have been conclusively identified by experiment. These points demonstrate that further work, employing powerful structural probes, is needed to increase the understanding of the incorporation of silicon in diamond. This is especially true in light of the recent demonstration that the 737 nm center, formed by implantation of silicon, has the potential to be a single photon source,[21] which could be exploited for applications such as quantum cryptography, quantum computation, and quantum optics.

B. Electron paramagnetic resonance centers correlated with silicon incorporation

Electron paramagnetic resonance (EPR) is an attractive experimental tool for the identification and characterization of defects in diamond, due to its high sensitivity and ability to extract information on both the constituents and the structure of paramagnetic defects.

A trigonal defect with $S=1$, referred to as KUL1, has been detected in CVD diamond films grown on silicon substrates.[22] The polishing of the substrate side led to a reduction in the intensity of the observed resonance lines, leading to the suggestion that the defect is silicon related. The $^3A_{2g}$ ground state of $(V\text{-Si-}V)^0$ is predicted[13] to be paramagnetic with $S=1$; hence, this model has been associated with KUL1.[23] As was found for the 737 nm defect, KUL1 is stable, surviving an annealing temperature of 1400 °C.[22]

The $(V\text{-Si-}V)^0$ model for KUL1 permits definite predictions to be made regarding the hyperfine structure of this defect. As apparent from Fig. 1, there are six equivalent nearest-neighbor carbon atoms and a single silicon atom. Both ^{13}C and ^{29}Si (with natural abundances 1.1% and 4.7%, respectively) have $I=\frac{1}{2}$; hence, satellites (centered on transitions from ^{28}Si, ^{30}Si, and ^{12}C defects) from the hyperfine interactions of these two isotopes would be expected. With an applied magnetic field $\underline{B}$ in the {110} plane, a maximum of three pairs of ^{13}C satellites and, since there is only one possible site for the ^{29}Si atom, a single pair of satellite lines from ^{29}Si would be observed. The previously reported experimental data concerning the hyperfine structure of KUL1[22,23] do not match the predictions of the $(V\text{-Si-}V)^0$ model. A tentative assignment of one pair of hyperfine satellites was made to ^{29}Si, but the remaining satellites did not suggest six equivalent carbon atoms; instead, a unique site and two equivalent sites were reported. Due to the apparent trigonal symmetry of KUL1, it is difficult to construct a defect that is consistent with the previously reported ^{13}C hyperfine structure.

It should also be noted that $(V\text{-Si-}V)^-$ would be expected to be paramagnetic, with the theoretical models suggesting that the ground state has $S=\frac{1}{2}$.[13,20] Another defect, labeled KUL8, has $S=\frac{1}{2}$ and has been detected in polycrystalline CVD material deposited on silicon substrates.[24,25] As for KUL1, KUL8 was found to be mainly incorporated close to the substrate, but since no hyperfine structure has been resolved it could not be conclusively identified as being silicon related and its symmetry could not be probed. Illumination at 457.9 nm of samples containing both KUL1 and KUL8 has suggested that the EPR intensity is transferred from one defect to the other.[24,25] Hence, it was proposed that the two features are different charge states of the same defect, with the assignment of KUL8 to $(V\text{-Si-}V)^-$. However, photochromism, by itself, does not permit identification of a defect.

Finally, there is the assignment of KUL3 to an $S=\frac{1}{2}$ defect of monoclinic-I (C_{1h}) symmetry.[22,23] The involvement of hydrogen was inferred due to the presence of weak satellites around the principal lines, which could be assigned to the forbidden proton nuclear-electron double spin-flip transitions.[22] A correlation between the silicon content and the concentration of KUL3 was determined; in a single-crystal film that showed a variation of the intensity of the 737 nm system, the intensity of KUL3 was found to be highest in the most silicon-rich parts. A proposed model is that the center is associated with a neutral divacancy, where one of the six basal carbon atoms is replaced by silicon and one dangling bond (remote to the silicon atom) is passivated by a hydrogen atom.[23] This model is not supported by recent theoretical predictions from Goss *et al.*,[20] who assigned KUL3 to $(V\text{-Si-}V)^0$ decorated with a nearby hydrogen atom, which will be referred to in this text as $(V\text{-Si-}V\text{:H})^0$.

C. Controlled doping of charge vapor deposited diamond with silicon

Improved control in CVD synthesis has enabled the growth of diamond without observable silicon or nitrogen contamination (e.g., no 737 nm system observed in PL). Controlled doping of diamond with silicon is therefore possible, which can be achieved via the addition of silane (or other silicon-containing gas) to the growth gases.[26]

Doping experiments have indicated that, although the probability of silicon incorporation into bulk homoepitaxial diamond via a major {100} growth surface from the gas phase is less that that of boron, it is more efficiently incorporated than nitrogen.[26] To date, no information is known regarding the relative incorporation efficiency of silicon on the {110} or {111} diamond surfaces. It has also been demonstrated that the presence of silicon in the source gases can have a dramatic effect on the optical properties of the diamond deposited, especially when nitrogen is present in the growth environment.[26]

In this paper, we present data obtained by multifrequency continuous-wave EPR on SC-CVD diamond samples that have been deliberately doped with silicon via the method outlined above. Isotopic enrichment of the samples was used to unambiguously identify silicon as a constituent of the defects studied via observations of the ^{29}Si hyperfine structure. Analysis of the orientation dependence and relative intensities of the ^{13}C and ^{29}Si hyperfine satellites have enabled conclusive determination of defect symmetries and structures.

II. EXPERIMENT

The SC-CVD diamond samples used for the studies presented here have been homoepitaxially grown on {100} or {110} oriented single-crystal diamond substrates and were doped with silicon by the addition of silane to the growth gases. Silane containing ^{29}Si in natural abundance (4.7%) or enriched to 90% (supplied by Voltaix, Inc., USA) was used in a series of growth runs. After deposition, the substrates were removed to leave freestanding plates, which were then cut and polished to remove twinned and poor quality material from the edges.

PL measurements were made using a commercial Renishaw inVia Raman microscope with an argon ion laser (514.5 nm) at temperatures down to 4 K in a continuous flow cryostat (Oxford Instruments LHe microstat). UV, visible, and near-infrared (NIR) absorption measurements were obtained using a Perkin Elmer Lambda 19 spectrometer with a 0.7 mm aperture, with the sample at ~90 K in a liquid nitrogen cryostat.

Room temperature EPR measurements have been performed on these samples using a commercial Bruker *X*-band (9.7 GHz) spectrometer equipped with a Super-High-*Q* (ER4122SHQ) cavity and a custom-built *Q*-band (35 GHz) spectrometer, previously described by Twitchen *et al.*[27] Both systems have been set up to enable a sample to be rotated in two perpendicular planes, allowing the positions of the observed resonances lines to be investigated, as a function of angle, in any given crystallographic plane. In the case of the *X*-band spectrometer automated rotation studies are possible using a stepper motor controlled goniometer. Low-temperature (down to 7 K) measurements were conducted using an *X*-band spectrometer equipped with a continuous flow cryostat (Oxford Instruments ESR900) and a TE_{104} (Bruker ER4105DR) cavity.

The concentrations of all paramagnetic defects found in the examined samples have been determined by EPR. When conducting quantitative EPR measurements of defects in diamond, care must be taken to avoid microwave saturation; hence, in this study, *X*-band EPR spectra at various powers between 0.2 nW and 3 mW were used in order to negate this problem. EPR spectra are recorded using magnetic field modulation (resulting in a spectrum that approximates the first derivative of the EPR line shape); therefore, double integration is required to determine the EPR intensity. The defect concentration can then be determined by comparing the intensity to that from a reference sample of known concentration. A single growth sector HPHT synthetic Ib diamond that contains 240 ± 20 ppm carbon atoms of $(N_s)^0$, was used in this study.

Since the spectral features from many paramagnetic defects occur around $g=2$, to determine the integrated intensity it is often necessary to deconvolve overlaying spectra; hence, a computer program to simultaneously fit a number of different overlapping spectra has been developed in house. Often neither a Lorentzian nor a Gaussian line shape provides a good fit to the experimental EPR spectra; a Tsallis[28] function is used to produce the simulated spectra. Furthermore, in the case of low defect concentrations, it is often necessary to use modulation amplitudes approaching or exceeding the linewidth of the EPR signals to achieve an adequate signal/noise ratio (enabling accurate concentration determination within a reasonable time frame). Hence, pseudomodulation[29] is employed, in combination with the Tsallis line shape, in order to produce the best fit to the experimental data. The deconvolved fit to each paramagnetic defect present is then used to calculate the concentration of that center by double integration. Repeated measurements and the quality of fit are used to estimate the errors in the determined defect concentrations.

Fourier transform infrared (FTIR) absorption measurements were taken using a PerkinElmer Spectrum GX spectrometer equipped with a beam condenser. Spectra were taken over the midinfrared region at a resolution of 1 cm^{-1}. All measurements were made at room temperature. Analysis of the absorption spectra enabled the concentration of $(N_s)^+$ to be estimated using the previously determined absorption coefficient[30] [5.5 ± 1 ppm of $(N_s)^+$ gives rise to an absorption coefficient of 1 cm^{-1} at 1332 cm^{-1}].

III. RESULTS

A. Sample characterization

Sample A was grown on a {110} oriented substrate and doped with silicon using silane containing the natural abundances of silicon isotopes. Samples B and C were grown with the addition of silane isotopically enriched to 90% ^{29}Si. Sample B was grown on a {100} substrate, while a {110}

TABLE I. Summary of the quantitative results obtained regarding the concentration of the major nitrogen-related defects and those thought to be silicon related. $(N_s)^0$, KUL1, and KUL3 concentrations were determined using EPR and $[(N_s)^+]$ was estimated using FTIR. In sample A, $(N_s)^+$ was below detection limits (~100 ppb). The concentrations that can be inferred from the integrated absorption of the 737 nm zero phonon line are discussed in Sec. IV A. The final column indicates the total silicon concentration, as determined by SIMS.

Sample	Substrate	$[(N_s)^0]$ (ppb)	$[(N_s)^+]$ (ppb)	[KUL1] (ppb)	[KUL3] (ppb)	737 nm (meV cm^{-1})	[Si] (ppb)
A	{110}	<0.5		100(10)	6(3)	0.93	~600
B	{100}	20(10)	~1200	30(5)	1.0(5)	24.1	
C	{110}	20(10)	~800	400(20)	5(2)	24.8	

oriented substrate was used for the growth of sample C. All three samples were examined after they were cut and polished.

The 737 nm line, observed in PL measurements, was found to be strong in all the samples examined. Comparing the EPR spectra to the published data on KUL1 and KUL3[23] revealed that both these centers were present in detectable concentrations in all three samples. KUL8, however, was not detectable in any of the samples examined. In samples B and C $(N_s)^0$ could also be readily detected by EPR, while in sample A no signal from $(N_s)^0$ could be detected; hence, only an upper limit can be quoted for the concentration in this sample.

An absorption at 1332 cm^{-1} was not detectable in sample A, but in samples B and C the absorption peak was sufficiently large to permit an estimation of the concentration of $(N_s)^+$. In both these samples, $[(N_s)^+]$ was on the order of 1 ppm; hence, $[(N_s)^+] \gg [(N_s)^0]$. Given the concentration of $(N_s)^0$ determined from EPR, it is not surprising that no absorption at 1130 cm^{-1} could be observed in any of the examined samples.[31]

Secondary ion mass spectroscopy (SIMS) measurements on sample A were conducted to measure the concentration of silicon. An average over the sample of approximately 600 parts per 10^9 (ppb) carbon atoms was determined, but it should be noted that the local concentration varied by more than a factor of 6.

Table I summarizes the concentrations obtained from the EPR, FTIR, and SIMS measurements, as well as the integrated absorptions for 737 nm (detected in the optical absorption measurements). The results presented in Table I will be discussed in Sec. IV A, wherein information that these data provide regarding the incorporation of silicon in diamond is covered.

Since both KUL1 and KUL3 were present in readily detectable concentrations in all three samples, further investigation of these defects by EPR was possible.

B. KUL1

To investigate the orientation dependence of the main KUL1 EPR lines, spectra were obtained at 5° increments from $\theta=0°$ (parallel to [001]) to $\theta=90°$ (parallel to [110]), equating to a rotation of the applied magnetic field ($\underline{B}$) in the $(1\bar{1}0)$ plane. The positions of the observed resonance lines in the ^{28}Si sample (A) at *X*-band frequencies as a function of the angle are plotted in Fig. 2. The lines are labeled i–vi to aid future referencing.

A number of hyperfine pairs were visible around each KUL1 resonance line. To view the effect that isotopic enrichment with ^{29}Si has on the hyperfine structure, narrow scans, with $\underline{B} \| \langle 111 \rangle$, were obtained around the KUL1 resonance lines for the sample containing 4.7% ^{29}Si and those enriched to 90%. Figure 3 shows the hyperfine structure around line i. Figure 3 establishes that the outermost satellites can be assigned to a ^{29}Si hyperfine interaction, with the ratio of the intensity of these satellites to the central line in Fig. 3 equal to ~9:1, in agreement with the quoted enrichment of the silane. These findings confirm the involvement of silicon in this defect. The remaining pair of satellites were assigned to ^{13}C since they evidently arise from an $I=\frac{1}{2}$ isotope with a low natural abundance (^{13}C is 1.1% abundant).

To examine the orientation dependence of these hyperfine satellites and to determine the number of equivalent positions for ^{29}Si and ^{13}C atoms in this defect, scans at both *X*- and *Q*-band frequencies were made with $\underline{B}$ at different orientations in the $(1\bar{1}0)$ plane. Rotating away from $\langle 111 \rangle$ revealed that the ^{29}Si satellites did not split, while the ^{13}C satellites split into a maximum of two sets around the lines

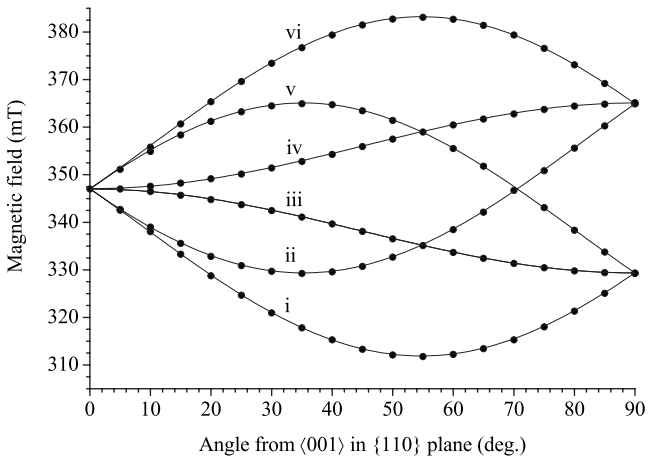

FIG. 2. The points indicate the determined positions, as a function of angle in the $(1\bar{1}0)$ plane of the KUL1 EPR lines at *X*-band frequencies. The solid curves show the best fit to the experimental data and were used to determine the parameters *g* and *D* (see text).

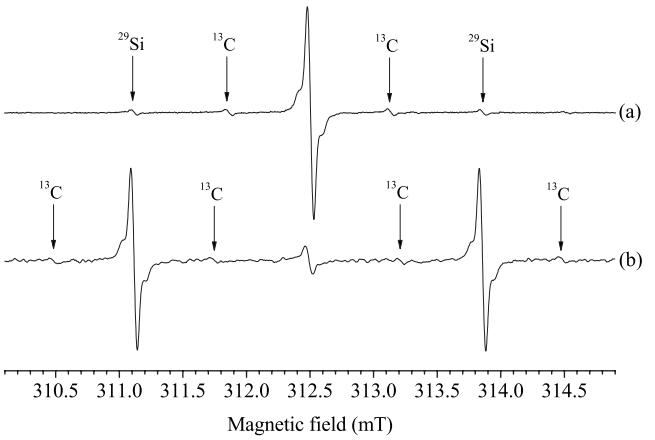

FIG. 3. A comparison between the KUL1 hyperfine structures observed around line i (see Fig. 2) (a) for a sample with ^{29}Si in its natural abundance and (b) for one enriched to 90% ^{29}Si. The spectra were recorded at X-band frequencies with $\underline{B}\|\langle 111\rangle$.

labeled i, ii, v, and vi in Fig. 2 and three sets around the lines labeled iii and iv in Fig. 2. Figure 4 shows an example of the hyperfine structure observed at X-band frequencies with the applied magnetic field 80° from [001] in the $(1\bar{1}0)$ plane for the sample containing ^{29}Si in its natural abundance. The lines labeled $^{29}\mathrm{Si}_a$ and $^{13}\mathrm{C}_{a-c}$ are not observed in Q-band measurements (see Sec. IV B). The orientation dependence in the $(1\bar{1}0)$ plane of the lines assigned to ^{13}C and ^{29}Si satellites are plotted in Fig. 5.

In order to investigate the effect of temperature on the KUL1 resonance lines, X-band spectra were obtained at a number of temperatures between 10 and 300 K, with $\underline{B}\|\langle 111\rangle$. Between 300 and 30 K, the splitting of the outermost KUL1 resonance lines was seen to decrease from 71.2(1) mT at 300 K to 67.4(1) mT at 30 K. Over this temperature range, the linewidth was constant and the intensity of the spectrum was seen to follow Curie's law; i.e., it was proportional to T^{-1}. Below 30 K the, intensity of KUL1 rapidly decreased, as microwave power saturation became unavoidable, with 0.3 μW being the lowest microwave power achievable with the setup used for cryogenic temperature EPR (see Sec. II). EPR lines from KUL1 could still be observed below 30 K but only under rapid passage conditions, making quantitative measurements impossible. No changes in symmetry were apparent at reduced temperatures.

C. KUL3

Narrow EPR scans around $g=2$ were obtained at ~5° increments in the $(1\bar{1}0)$ plane for sample A at both X- and Q-band frequencies to permit a roadmap of the KUL3 resonance lines to be constructed. From Table I, it is apparent that KUL3 is present in much lower concentrations than KUL1; hence, close to $\langle 100\rangle$, the resonance lines from KUL1 dominated the spectra, meaning the positions of the KUL3 lines could not be accurately determined. Figure 6 illustrates the road maps constructed from sample A (4.7% ^{29}Si).

Small pairs of hyperfine satellites were observed around the central KUL3 resonance lines in sample A. Hence, in

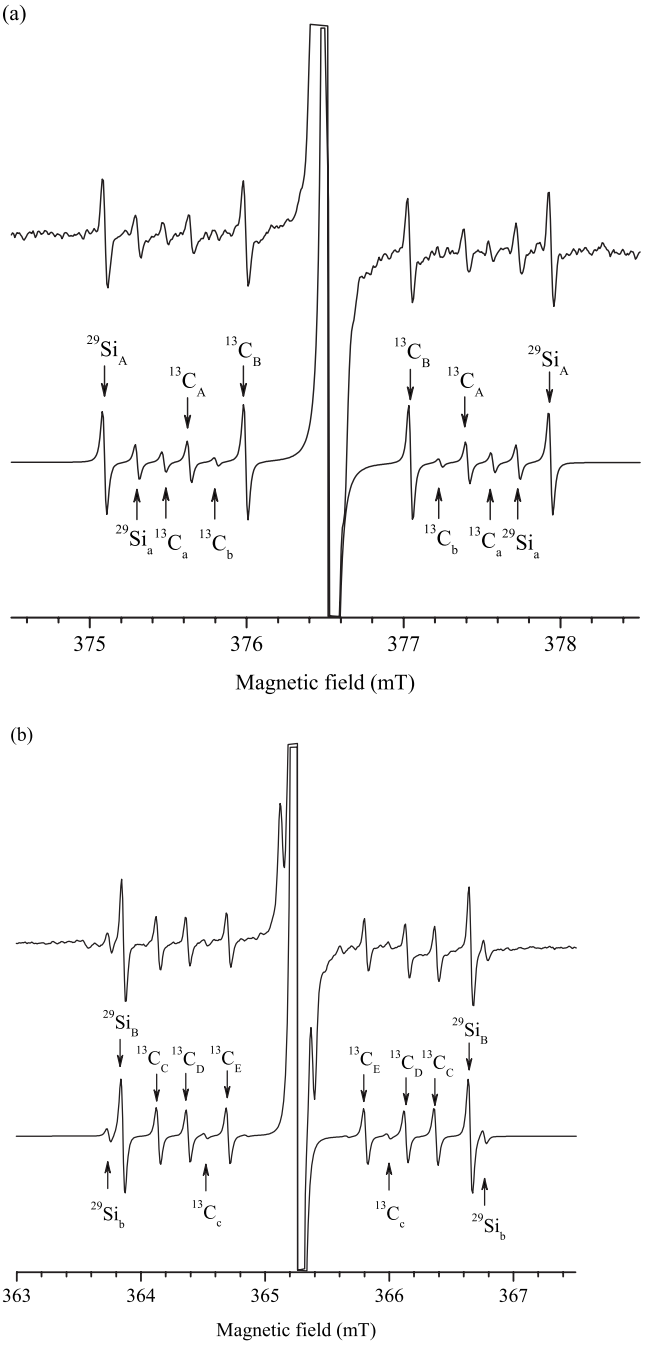

FIG. 4. KUL1 hyperfine structure observed at X-band frequencies with $\theta=80°$ in the $(1\bar{1}0)$ plane. The plots beneath illustrate the simulated data obtained using the determined spin-Hamiltonian parameters and Eqs. (1) and (2). The lowercase labels denote lines that are absent in Q-band spectra. (a) Displays the structure around resonance line vi and (b) shows the hyperfine satellites seen around line iv (see Fig. 2).

order to assist in their identification, identical X- and Q-band scans were obtained for the samples containing 4.7 and 90% ^{29}Si (samples A and B, respectively). The effect of enrichment is shown in Fig. 7, which shows the X-band EPR spectra with $\underline{B}\|\langle 111\rangle$. Since the intensity of the satellites is increased such that the ratio of intensity of these to the center line is 9:1, this unambiguously identifies these as ^{29}Si hyper-

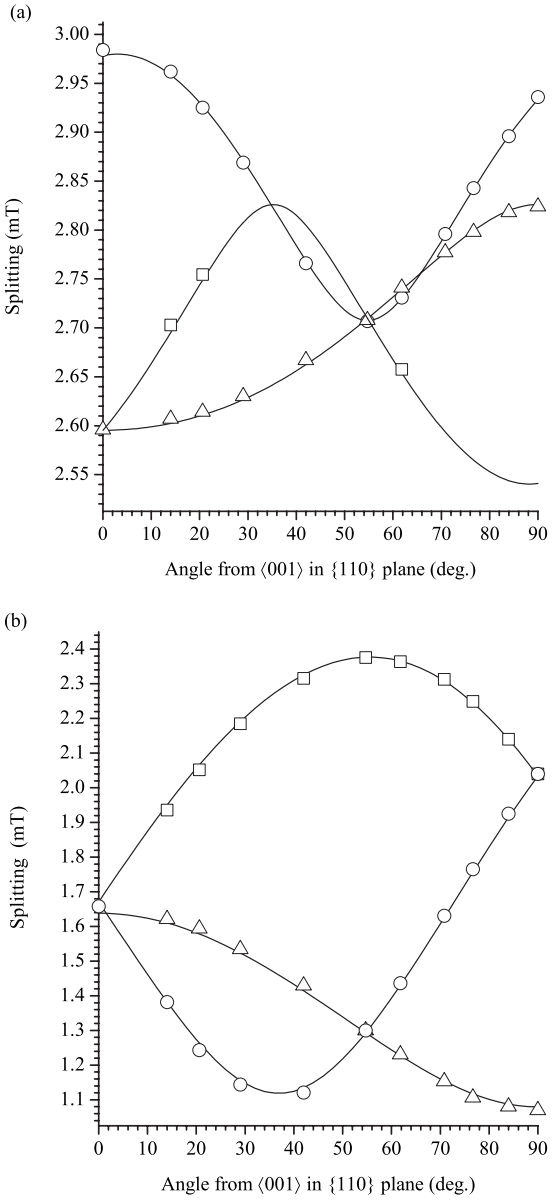

FIG. 5. (a) Splitting of the ^{29}Si hyperfine satellites around KUL1 resonance lines i (□), ii (△), and iii (○) (see Fig. 2) as a function of angle in the $(1\bar{1}0)$ plane. (b) Splitting of the ^{13}C satellites as a function of angle in the $(1\bar{1}0)$ plane. The three data sets (○, △, and □) illustrate the splitting of satellites $^{13}C_A/^{13}C_C$, $^{13}C_B/^{13}C_E$, and $^{13}C_D$, respectively (see Fig. 4). The error bars are comparable to the size of the data points. The plotted lines were created using the spin-Hamiltonian parameters and Eqs. (1) and (2).

fine satellites and confirms the presence of silicon in this center. A number of spectra at different orientations in the $(1\bar{1}0)$ plane were obtained for the ^{29}Si enriched samples to permit the ^{29}Si hyperfine parameters to be determined.

IV. DISCUSSION

A. Incorporation of silicon in diamond

It is known that the intensity of the 737 nm silicon-related absorption system can be dramatically increased by irradiation damage and annealing at temperatures where vacancies are mobile. This result supports the assignment of the 737 nm defect to a (*V*-Si-*V*) structure and the incorporation of silicon in another form that is converted to (*V*-Si-*V*) by vacancy capture.

The SIMS data in Table I indicate that more silicon is incorporated in sample A than is accounted for by the EPR defects KUL1/KUL3. As stated in Sec. III A, the silicon incorporation is highly inhomogeneous and this will be discussed in future publications. Optical absorption intensities are reported for the 737 nm doublet; but because of the lateral inhomogeneity in the silicon concentration of these samples, these measurements should be treated with caution.

The conversion factor relating the absorption intensity under the zero phonon line at 77 K (A_{737}) in units of meV cm^{-1} to a concentration ([737]) in cm^{-3} is not known; however, an estimation can be made by considering the data from other defects in diamond. A typical conversion factor[32] at 77 K is $\sim 2\times 10^{16}$ meV cm^2 for defects with a Huang–Rhys factor (which is a measure of the vibronic coupling) of ~ 3.[33] Using the published value of 0.05 for the Huang–Rhys factor of the 737 nm system,[34] one would expect the conversion factor for this defect to be a factor of ~ 60 higher; $\sim 10^{18}$ meV cm^2. In this way, we can crudely estimate the concentration of the defect giving rise to the 737 nm system from the data in Table I using the expression $A_{737}=10^{18}[737]$. A concentration of ~ 1 ppb is estimated for sample A and ~ 12 ppb for samples B and C (1 ppb equates to a defect density of 1.77×10^{14} cm^{-3}).

Due to the very low concentration of nitrogen in sample A, one would expect the majority of silicon defects to be neutral. Using our concentration estimates, we find a significantly higher ratio of [KUL1] to [737] in this sample compared to both samples B and C, which contain much more nitrogen. However, despite samples B and C being grown under identical conditions, it appears that the ratio of [KUL1] to [737] is different between the two samples. Although the concentration of $(N_s)^+$ obtained from FTIR should be treated with caution in the same way as the results inferred from the 737 nm absorption measurements, it appears that a higher proportion of the nitrogen in sample B is in the positive charge state, $(N_s)^+$. This could explain the higher fraction of [737] in this sample compared to sample C.

The combined concentrations of KUL1, KUL3, and the 737 nm defect in samples B and C suggest that silicon, at least in these forms, is more readily incorporated on {110} growth surfaces than on {100}.

B. KUL1

The large splitting of the outermost KUL1 resonance lines observed with $\underline{B}\|\langle 111\rangle$ suggests that a zero-field splitting (D) is primarily responsible for the orientation dependence of the lines shown in Fig. 2, therefore implying that the defect has $S\geq 1$. Weak resonance lines, present at the half field originating from a $|-1\rangle\rightarrow|+1\rangle$ transition, and the absence of any lines from $|-\frac{1}{2}\rangle\rightarrow|+\frac{1}{2}\rangle$ transitions confirm that the defect has $S=1$. The Curie law variation of intensity with

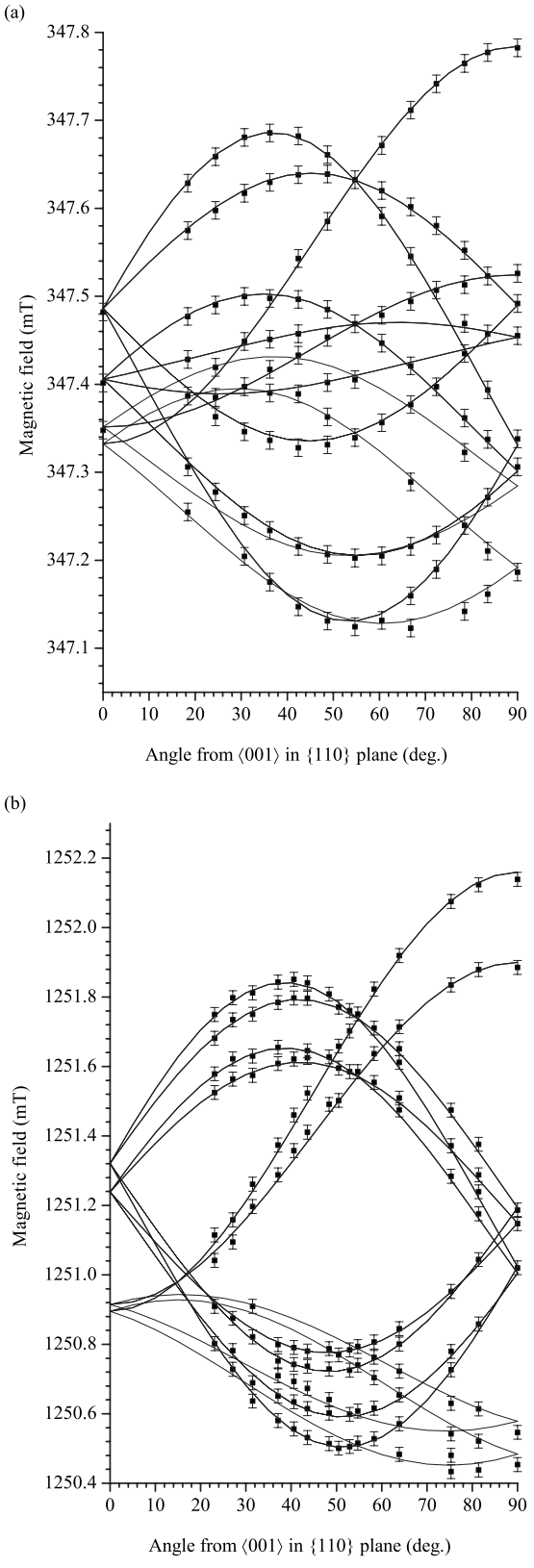

FIG. 6. The determined positions as a function of angle in the $(1\bar{1}0)$ plane of the KUL3 EPR lines observed at (a) X-band and (b) Q-band frequencies. The plotted lines were obtained using the determined parameters for g and A (see Table III).

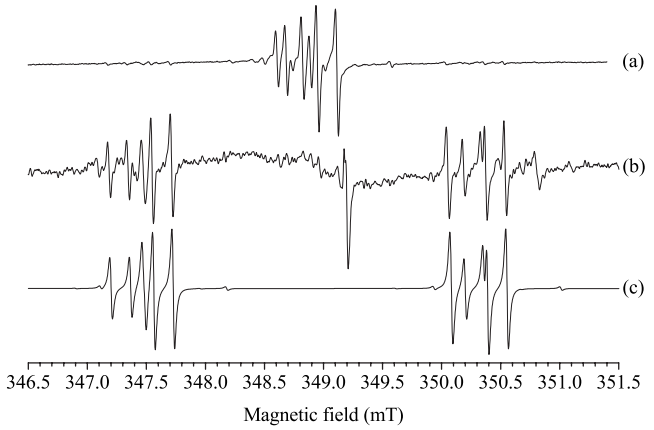

FIG. 7. EPR lines observed around $g=2$ at X-band frequencies with $\underline{B}$ along ⟨111⟩ for (a) sample A (^{29}Si in natural abundance) and (b) sample B (enriched with 90% ^{29}Si). The central resonance line in (b) arises due to the presence of $(N_s)^0$ in this sample. (c) Shows a spectrum simulated using the determined parameters for KUL3, given in Table III.

temperature shows that this is the ground state, which is well separated from any excited states.

The results of the angular variation study have therefore been fitted using a spin Hamiltonian in the form of the following equation and the temperature dependence of the large splitting of the lines could be interpreted as a change in the magnitude of D:

$$H_{\text{electronic}} = \mu_B \underline{B} \cdot \underline{\mathbf{g}} \cdot \underline{S} + \underline{S} \cdot \underline{\mathbf{D}} \cdot \underline{S}. \quad (1)$$

Using the experimentally observed positions of the resonance lines, optimum values for the electronic Zeeman ($\underline{\mathbf{g}}$) and zero-field ($\underline{\mathbf{D}}$) terms could be found. It was assumed that $\underline{\mathbf{g}}$ and $\underline{\mathbf{D}}$ are axially symmetric about the [111] trigonal axis of the defect; relaxing this constraint did not improve the quality of the fit. The parameters for $\underline{\mathbf{g}}$ were determined relative to g for $(N_s)^0$, which was taken to be $g=2.0024$.[35] $g_\parallel$ and $g_\perp$ for KUL1 were found to be equal to 2.0042(2) and 2.0035(1), respectively, with $g_\parallel$ along [111]. The magnitude of the zero-field interaction D (where D is defined as $\frac{3}{2}D_{zz}$) was determined to be +1000(1) MHz at 300 K, again with the principal axis along [111] (note that 1 MHz $\sim$0.036 mT for $g=2.0023$). These results are in agreement with those previously published for KUL1.[23] Figure 8 illustrates the determined dependence of D on temperature.

From the change in the intensity of the outmost hyperfine satellites in samples enriched with ^{29}Si (see Fig. 3), it was apparent that these could be assigned to ^{29}Si. The splitting of this pair with orientation, illustrated in Fig. 5(a), can be used to extract the hyperfine (A) parameters, using an additional term in the spin Hamiltonian,

$$H_{\text{nuclear}} = \sum_j (\underline{S} \cdot \underline{\mathbf{A}}_j \cdot \underline{I}_j - \mu_N g_{N_j} \underline{B} \cdot \underline{I}_j), \quad (2)$$

where g_{N_j} is the nuclear g factor (g_N) for nuclei j.

The hyperfine interaction for ^{29}Si was found to be axially symmetric, with $A_\parallel$ oriented along the [111] trigonal axis (see Table II), although it should be noted that the orientation

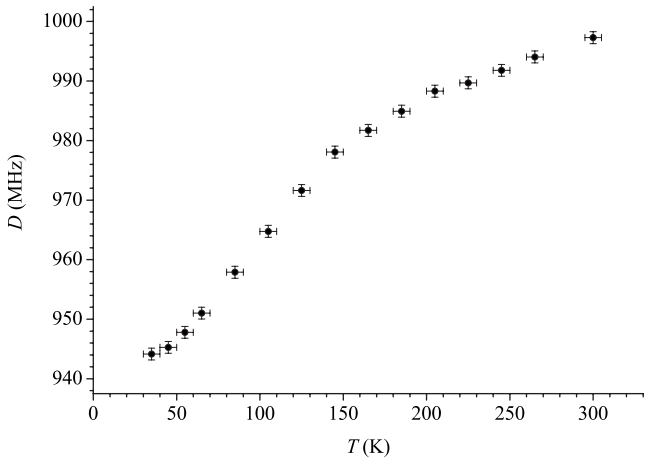

FIG. 8. The magnitude of the zero-field (D) interaction for KUL1 as a function of temperature. Note that 1 MHz $\sim$0.036 mT for $g=2.0023$.

dependence illustrated in Fig. 5(a) is dominated by the second order terms in D. Since the ^{29}Si satellites did not split when the orientation of $\underline{B}$ was changed, it is apparent that a single silicon atom is incorporated in the defect at a unique site. A silicon atom at the center of a divacancy, as in (V-Si-V), would explain the observed hyperfine symmetry and the single observable site. The data in Fig. 2 are consistent with a defect that has either D_{3d} or C_{3v} symmetry and, in itself, is insufficient to confirm the $(V\text{-Si-}V)^0$ model. The data obtained in Sec. III B are therefore important since the intensity of ^{13}C satellites relative to the central transition allows the number of equivalent atom positions to be determined. A defect with C_{3v} symmetry would have two distinct sets of three equivalent carbon atoms, with the addition of the inversion symmetry in $(V\text{-Si-}V)^0$ increasing the symmetry to D_{3d}, leading to a set of six equivalent carbon atoms (see Fig. 1).

For nuclei with abundance P and equivalent positions N, the intensity of the hyperfine satellites (Ω_{hf}) can be related to the intensity of the central line (Ω_{central}) by

$$\Omega_{\text{hf}} = N \times \frac{P}{1-P} \times \Omega_{\text{central}}. \tag{3}$$

The intensity of the simulated data in Fig. 4 has been set using Eq. (3), assuming that there are six nearest-neighbor carbon atoms ($N=6$), with ^{13}C being present in its natural abundance ($P=0.011$). A good match to the experimental data is found, confirming that KUL1 has D_{3d} symmetry, supporting the assignment of KUL1 to $(V\text{-Si-}V)^0$. The orientation dependence data for the ^{13}C satellites [Fig. 5(b)] was used to extract the hyperfine parameters for this interaction (see Table II). $A_{\parallel}$ was found be directed along the $\langle 111\rangle$ axis, which is not parallel to the D_{3d} symmetry axis (e.g., $[\bar{1}\bar{1}1]$); with the silicon atom located along [111], this result is as expected for the (V-Si-V) model.

The distributions in intensity between the ^{13}C hyperfine satellites illustrated in Fig. 4 can be explained using the $(V\text{-Si-}V)^0$ model, considering all the possible $\langle 111\rangle$ orientations of this defect. When the applied magnetic field $\underline{B}$ is rotated in the $(1\bar{1}0)$ plane in Fig. 1 (trigonal symmetry axis in the plane containing $\underline{B}$), four of the possible orientations of $A_{\parallel}$, arising from a ^{13}C atom at positions i, j, l, m, make the same angle with $\underline{B}$. A different angle is made by the other two possible orientations of $A_{\parallel}$, arising from ^{13}C at positions k or n. Hence, ^{13}C satellites for $(V\text{-Si-}V)^0$ defects along [111] would be expected to split with relative intensities of 4:2. For defects oriented along different $\langle 111\rangle$ orientations, a splitting into three pairs with intensities of 2:2:2 would arise. This is the behavior observed in Figs. 4(a) and 4(b), respectively.

It was noted in Sec. III B that the lines labeled $^{29}\text{Si}_{a\text{-}b}$ and $^{13}\text{C}_{a\text{-}c}$ were not observed in Q-band measurements. These could therefore be assigned to the *forbidden* electron-nuclear double-spin-flip ($\Delta M_S=1, \Delta m_I=1$) transitions. While their addition complicates the initial interpretation of the spectra, their positions relative to the allowed lines depend on the value of g_{N_j}, therefore allowing the isotope responsible to be identified. The good fit to the experimental data therefore further supports the assignment of the hyperfine structure to ^{29}Si and ^{13}C. These transitions are also sensitive to the relative signs of A and D. The absolute sign of D can be determined via depopulation of the higher energy spin states at lower temperatures. However, as stated in Sec. III B, below 30 K saturation became a problem; hence this was not possible. Nevertheless, providing assumptions are made regarding the unpaired electron wave-function localization the signs of D as well as A for the ^{29}Si and ^{13}C hyperfine interactions can be found via position of lines resulting from the electron-nuclear double-spin-flip transitions.

In previously published work[23] on KUL1, wherein it was initially proposed that KUL1 could be $(V\text{-Si-}V)^0$, the sign of the zero-field interaction was assumed to be negative, presumably to agree with the finding that $D<0$ for the divacancy in diamond.[36] Assigning KUL1 to $(V\text{-Si-}V)^0$ means

TABLE II. Experimentally determined (at 300 K) ^{13}C and ^{29}Si hyperfine (A) parameters for KUL1, compared to those predicted from theory (Ref. 20). Note that 1 MHz $\sim$0.036 mT for $g=2.0023$.

Interaction	$A_{\parallel}$ (MHz) [hkl]	$A_{\perp}$ (MHz)	A_s (MHz)	A_p (MHz)	η^2	λ
^{13}C (experiment)	66.2(2)$\parallel[\bar{1}\bar{1}1]$	30.2(2)	42.2(1)	12.3(1)	0.123(6)	10.0(7)
^{13}C (theory)	51$\parallel[\bar{1}\bar{1}1]$ (2°)	12	25	13	0.13	18
^{29}Si (experiment)	76.3(1)$\parallel$[111]	78.9(1)	78.0(1)	−0.87(5)		
^{29}Si (theory)	78$\parallel$[111]	82	81	−1		

that a real localization of the electron probability density on the basal carbon atoms is expected. Since g_N is positive for ^{13}C, this necessitates a positive value for A. D must be positive to successfully match the experimentally observed positions of the satellites labeled $^{13}C_{a\text{-}c}$ in Fig. 4. Using this sign for D also requires the ^{29}Si hyperfine interaction to be positive to correctly predict the positions of the $^{29}Si_{a\text{-}b}$ resonance lines.

The ^{13}C hyperfine interactions can be interpreted in the usual way in terms of an unpaired electron wave function,

$$\Phi = \sum_i \eta_i(\alpha_i\phi_{2s} + \beta_i\phi_{2p}), \tag{4}$$

where the summation is over the atoms on which the unpaired electron is localized and ϕ_{2s} and ϕ_{2p} are the $2s$ and $2p$ atomic orbitals, respectively. The parameters α_i, β_i, and η_i, taken to be real, are deduced following the standard procedure from the hyperfine parameters and atomic parameters tabulated by Morton and Preston.[37] The hybridization ratio is $\lambda \equiv (\beta_i/\alpha_i)^2$. The experimental wave-function parameters determined for ^{13}C are given in Table II. Approximately 75% of the unpaired electron probability density is located on the six nearest-neighbor carbon atoms. It is also apparent in Fig. 4(b) that there are additional hyperfine satellites that are partially resolved around the central KUL1 resonance line. These are likely to arise from next nearest-neighbor ^{13}C atoms, hence accounting for some of the remaining unpaired electron probability density.

The nuclear g factor for ^{29}Si is negative:[38] therefore, the determined positive hyperfine interaction implies a *negative* spin density at the nucleus. This suggests an indirect interaction (e.g., configuration interaction[39] and exchange polarization[40]) is responsible for the observed hyperfine interaction. Taking $a_0 = -4594$ MHz for the $3s$ orbital,[37] the isotropic part of the ^{29}Si hyperfine interaction could be produced by ~2% $3s$ character. A similar result was found for the tin-vacancy complex in silicon.[14]

A recent theoretical study by Goss *et al.*[20] provided estimations for the hyperfine interactions for ^{29}Si and ^{13}C in $(V\text{-Si-}V)^0$. The ^{29}Si interaction was predicted to be axial along [111] and is dominated by the isotropic component; $A_\parallel = 78$ and $A_\perp = 82$ MHz, in excellent agreement with the determined values. The ^{13}C interaction for the six nearest-neighbor carbon atoms was also predicted to be axial and within 2° of ⟨111⟩. Values of $A_\parallel = 51$ and $A_\perp = 12$ MHz were calculated. The localization of the unpaired electron probability density on each ^{13}C (η^2) calculated from the experimentally determined hyperfine parameters is in good agreement with theory, although the ratio between the localization in the s and p type orbitals differs.

The shift of the g value from the free-spin value g_e and the anisotropy for KUL1 is large ($\delta g_\parallel = 0.0019$) compared to most defects in diamond. This arises from a spin-orbit admixture of excited states, which, in a free atom, leads to a contribution to D of the form $D = \frac{1}{2}\lambda_{so}\delta g/g_e$, where λ_{so} is the spin-orbit coupling constant. Assuming $\lambda_{so} \sim 4.5 \times 10^5$ MHz for a carbon atom in an $S=1$ defect,[41] the contribution to D in KUL1 from the spin-orbit coupling is ~640 MHz. A more detailed analysis of the size of the zero-field splitting is complicated and will not be discussed further here, although the simple estimate shows that the large positive value of D can be explained by the spin-orbit coupling. We also note that in previous studies of KUL1, the magnitude of D was found to linearly increase with temperature in the range 10–300 K.[22] The dependence determined in this study, shown in Fig. 8, indicates a more complicated behavior that deserves further investigation.

C. KUL3

The orientation dependence of KUL3 resonance lines, shown in Fig. 6, indicates a defect with C_{1h} (monoclinic-I) symmetry with small splittings around $g=2$, implying that $S = \frac{1}{2}$. The weak hyperfine satellites visible in the sample containing ^{29}Si in its natural abundance suggest a low abundance $I = \frac{1}{2}$ nucleus is involved, with the data in Fig. 7 for a ^{29}Si enriched sample confirming that these arise from the presence of ^{29}Si. The intensity of the hyperfine satellites in the unenriched samples, relative to the central KUL3 resonance lines indicate that the satellites arise from a unique ^{29}Si atom. $\underline{\mathbf{A}}$ for ^{29}Si was found to be non-axial, with A_1 tilted approximately 2° away from [111] (toward [001]) in the $(1\bar{1}0)$ plane; constraining $\underline{\mathbf{A}}$ to be axial along [111] led to a statistically significant degradation in the quality of the fit. To produce the central pattern of resonance lines, another $I = \frac{1}{2}$ nucleus must be involved, with ~100% abundance. Due to its prevalence in CVD diamond growth, hydrogen is a natural choice, with the assignment being confirmed by the observation of electron-nuclear double-spin-flip transitions, as found in previous studies.[22]

From the road map for KUL3 (Fig. 6), the values describing $\underline{\mathbf{g}}$, as well as $\underline{\mathbf{A}}$, for the hydrogen atom were determined. The principal values of $\underline{\mathbf{g}}$ were found to be along [110], $[00\bar{1}]$, and $[1\bar{1}0]$. Allowing these to deviate from these directions did not improve the fit. The hydrogen hyperfine interaction is also nonaxial and is tilted ~4° from $[\bar{1}\bar{1}1]$ toward [001] in the $(1\bar{1}0)$ plane. Due to the low abundance of ^{13}C and the low concentration of KUL3, the hyperfine parameters for nearest- or next- nearest-neighbor ^{13}C could not be determined.

Table III provides a comparison of the spin-Hamiltonian parameters determined in this study and those previously published.[23] It is apparent that there is disagreement between the two. Using the previous parameters for KUL3 to fit the experimental X band data points in Fig. 6 resulted in a poor fit. This can be explained by the fact that these parameters were determined at Q-band frequencies. Since the g anisotropy of this defect is relatively large [cf. $(V\text{-Si-}V)^0$], at higher frequencies the changes in the positions of the resonance lines as the direction of $\underline{B}$ is changed will be dominated by this term in the spin Hamiltonian. By contrast the hyperfine term from the hydrogen atom will have a relatively small effect; hence, it is challenging to accurately determine at this frequency band. Additionally, it had previously been assumed that the principal axes for both g and A were along the same direction, which, as shown in Table III, is not the case if the directions of the two interactions are allowed to

TABLE III. Comparison between the previously published parameters (Ref. 23) for KUL3 and those determined in this study (at 300 K). θ is the angle from [001], ϕ is angle from [100] in the (001) plane. The hyperfine (A) parameters are quoted in megahertz (1 MHz $\sim$ 0.036 mT for $g=2.0023$). In this study, the parameters for $\underline{\mathbf{g}}$ were determined relative to g for $(N_s)^0$, which was taken to be $g=2.0024$ (Ref. 35).

Parameter	Previously published $[\theta, \phi]$	Determined $[\theta, \phi]$
g_1	2.00506(3)‖[75,45]	2.0054(2)‖[90,45]
g_2	2.00426‖[165,45]	2.0048(2)‖[0,45]
g_3	2.00254‖[90,315]	2.0030(2)‖[90,315]
A_1 (^{29}Si)		$\pm$76.1(2)‖[53(1),45]
A_2 (^{29}Si)		$\pm$81.1(2)‖[143(1),45]
A_3 (^{29}Si)		$\pm$79.1(2)‖[90,315]
A_1 (^{1}H)	−2.8(6)‖[75,45]	$\mp$7.9(1)‖[50(1),225]
A_2 (^{1}H)	0‖[165,45]	$\pm$4.7(1)‖[140(1),225]
A_3 (^{1}H)	7.3‖[90,315]	$\pm$7.3(1)‖[90,315]

independently vary. The modified parameters, used in Fig. 6, provide an excellent fit to the EPR data at both microwave frequencies. An example fit to an X-band spectrum with $\underline{B}\|\langle 111\rangle$ is shown in Fig. 7.

It was suggested that KUL3 is a neutral divacancy, where one of the six basal carbon atoms is replaced by silicon and one dangling bond (remote to the silicon atom) is passivated by a hydrogen atom.[23] The data obtained in this study confirm the involvement of hydrogen and silicon in this defect, but the new experimental data and a recent theoretical modeling[20] of hydrogen in the vicinity of (Si_s-V) both imply an alternative structure; $(V\text{-Si-}V\text{:H})^0$.

The magnitude of the ^{29}Si hyperfine parameters determined for KUL1 and KUL3 in this study are almost identical, but KUL3 has a lower symmetry. This suggests that the silicon atom is in a similar environment; the basic (V-Si-V) unit is common to both defects, but KUL3 is decorated with a single hydrogen atom (V-Si-V:H). The determined directions for the hyperfine interactions for ^{29}Si is consistent with this assignment, as the principal axis is close to the [111] axis containing the divacancy, as found for KUL1. This is in agreement with the theoretical predictions for the (V-Si-V:H) center, a stable defect with C_{1h} symmetry where the hydrogen atom is bonded close to the relaxed (V-Si-V) structure.[20]

The absolute sign of the hyperfine parameters for ^{29}Si and ^{1}H for $(V\text{-Si-}V\text{:H})^0$ could not be experimentally determined by EPR, although A for the ^{29}Si interaction is likely to be positive, in agreement with the sign determined for $(V\text{-Si-}V)^0$. Theoretical predictions for the ^{29}Si hyperfine interaction support this with A_1, A_2, and A_3 all determined to be positive.[20] The theoretically calculated ^{29}Si hyperfine interaction is within 3° of [111], in the $(1\bar{1}0)$ plane, in good agreement with the value determined from experiment. The predictions from theory for the magnitudes for the hydrogen hyperfine interaction ($A_1=-7$ MHz, $A_2=3$ MHz, and $A_3=6$ MHz) are also in good agreement with the values from EPR and are consistent with the localization of the unpaired electron probability density on the surrounding carbon atoms. Considering this model, the experimentally determined 5° deviation of A_1 from $[\bar{1}\bar{1}1]$ (toward [001]) for the hydrogen hyperfine interaction is reasonable.

V. CONCLUSIONS

EPR has been used to study defects present in SC-CVD samples deliberately doped with silicon by the addition of silane to the growth gases. We conclude that the EPR spectra for KUL1 are consistent only with a neutral silicon split-vacancy model, $(V\text{-Si-}V)^0$, and KUL3 has been shown to be the same defect but decorated with a hydrogen atom bonded in the vicinity of the $(V\text{-Si-}V)^0$ structure, $(V\text{-Si-}V\text{:H})^0$, as proposed by Goss *et al.*[20] These models were confirmed from the intensities and orientation dependence of the ^{13}C and ^{29}Si hyperfine satellites in KUL1 and the ^{1}H and ^{29}Si hyperfine satellites for KUL3. In both defects the presence of silicon was proved by examining samples enriched with ^{29}Si; in such samples the intensity of the hyperfine satellites assigned to ^{29}Si increased, such that the ratio of these to the central (^{28}Si) resonance line matched the quoted isotopic enrichment of the silane used in the growth. There is excellent agreement between the hyperfine parameters determined for $(V\text{-Si-}V)^0$ and $(V\text{-Si-}V\text{:H})^0$ and those calculated using local density functional theory.[20]

The symmetry of the $\underline{\mathbf{g}}$ and $\underline{\mathbf{D}}$ matrices determined for KUL1 are consistent with the $(V\text{-Si-}V)^0$ model. Although a detailed interpretation of the magnitudes of these parameters has not yet been attempted, it has been shown that a simple spin-orbit coupling estimate of the magnitude of D from the g shift suggests that the zero-field interaction is dominated by this term. The observed temperature variation of the $\underline{\mathbf{D}}$ matrix is interesting and deserves further study.

The KUL8 defect, suggested[24,25] to be $(V\text{-Si-}V)^-$, has not been detected in any of the samples examined. To date no additional spectra have been observed by the authors of this paper that can be assigned to $(V\text{-Si-}V)^-$, despite the presence of absorption and /or PL features at 737 nm. The concentration of the 737 nm defect was estimated from the absorption measurements to be $\sim$12 ppb in two of the samples examined, which is well above the detection limit in EPR. Hence, the apparent absence of an EPR spectrum that can be attributed to the $S=\frac{1}{2}$ ground state of $(V\text{-Si-}V)^-$ is intriguing.

It is possible that the EPR spectra from the $(V\text{-Si-}V\text{:H})^0$ defect overlap with EPR lines from $(V\text{-Si-}V)^-$. It is apparent that additional, as yet unidentified, EPR lines are present in these samples (see, for example, Fig. 7, wherein an additional resonance line is observed at 350.8 mT). In a previous study, KUL3/$(V\text{-Si-}V\text{:H})^0$ has been observed to anneal out at 1400 °C, at the same time as another (likely hydrogen-related defect) was seen to increase in intensity.[22] Annealing studies are therefore planned to further investigate the stability of $(V\text{-Si-}V\text{:H})^0$ and to aid in the identification of any additional EPR spectra that remain or are formed during annealing.

The lack of detection of $(V\text{-Si-}V)^-$ may be due to dynamic Jahn–Teller splitting of the ground state, giving rise to an averaging between different configurations that is fast on the time scale of an EPR experiment. Such averaging could result in the ground-state EPR signal becoming very broad, hence making it hard to detect. Such an effect has recently been used to explain why the ground state of NV^0 has not been detected by EPR.[42] We note that the samples examined that have a high concentration of the 737 nm defect display a very broad signal (~ 1 mT) around $g=2$. This is absent in a sample that contained an order of magnitude lower concentration of this center. Applying uniaxial stress to the sample while conducting an EPR experiment could lift the degeneracy and allow the ground state to be detected. These studies are in progress.

ACKNOWLEDGMENTS

Chris Kelly of the DTC Research Centre, Maidenhead is thanked for invaluable help with sample preparation. A.M.E. would also like to thank the DTC Research Centre for an Industrial Bursary. We also gratefully acknowledge J. P. Goss for helpful discussions and S. Liggins for assistance with the FTIR measurements. This work was supported by the EPSRC-GB (Grant Reference No. GR/S96777/01).

*m.e.newton@warwick.ac.uk

[1] J. Isberg, J. Hammersberg, E. Johansson, T. Wikstrom, D. J. Twitchen, A. J. Whitehead, S. E. Coe, and G. A. Scarsbrook, Science **297**, 1670 (2002).
[2] A. T. Collins, in *Properties and Growth of Diamond*, edited by G. Davies (INSPEC, London, 1994), Chap. 9.7, p. 288.
[3] J. W. Vandersande, in *Properties and Growth of Diamond*, edited by G. Davies (INSPEC, London, 1994), Chap. 1.7, pp. 33–35.
[4] J. Barjon, E. Rzepka, F. Jomard, J. M. Laroche, D. Ballutaud, T. Kociniewski, and J. Chevallier, Phys. Status Solidi A **202**, 2177 (2005).
[5] P. Joeris, I. Schmidt, and C. Benndorf, Diamond Relat. Mater. **5**, 603 (1996).
[6] V. S. Vavilov, A. A. Gippius, A. M. Zaitsev, B. V. Deryaguin, B. V. Spitsyn, and A. E. Aleksenko, Sov. Phys. Semicond. **14**, 1078 (1980).
[7] A. M. Zaitsev, V. S. Vavilov, and A. A. Gippius, Sov. Phys. Lebedev. Inst. Rep. **10**, 15 (1981).
[8] G. Sittas, H. Kanda, I. Kiflawi, and P. M. Spear, Diamond Relat. Mater. **5**, 866 (1996).
[9] C. D. Clark, H. Kanda, I. Kiflawi, and G. Sittas, Phys. Rev. B **51**, 16681 (1995).
[10] C. D. Clark and C. B. Dickerson, Surf. Coat. Technol. **47**, 336 (1991).
[11] A. T. Collins, L. Allers, C. J. H. Wort, and G. A. Scarsbrook, Diamond Relat. Mater. **3**, 932 (1994).
[12] G. Davies, S. C. Lawson, A. T. Collins, A. Mainwood, and S. J. Sharp, Phys. Rev. B **46**, 13157 (1992).
[13] J. P. Goss, R. Jones, S. J. Breuer, P. R. Briddon, and S. Oberg, Phys. Rev. Lett. **77**, 3041 (1996).
[14] G. D. Watkins, Phys. Rev. B **12**, 4383 (1975).
[15] J. P. Goss, P. R. Briddon, R. Jones, and S. Sque, Diamond Relat. Mater. **13**, 684 (2004).
[16] J. P. Goss, P. R. Briddon, M. J. Rayson, S. J. Sque, and R. Jones, Phys. Rev. B **72**, 035214 (2005).
[17] A. T. Collins, M. Kamo, and Y. Sato, J. Mater. Res. **5**, 2507 (1990).
[18] S. W. Brown and S. C. Rand, J. Appl. Phys. **78**, 4069 (1995).
[19] H. Sternschulte, K. Thonke, J. Gerster, W. Limmer, R. Sauer, J. Spitzer, and P. C. Munzinger, Diamond Relat. Mater. **4**, 1189 (1995).
[20] J. P. Goss, P. R. Briddon, and M. J. Shaw, Phys. Rev. B **76**, 075204 (2007).
[21] C. L. Wang, C. Kurtsiefer, H. Weinfurter, and B. Burchard, J. Phys. B **39**, 37 (2006).
[22] K. Iakoubovskii and A. Stesmans, Phys. Status Solidi A **186**, 199 (2001).
[23] K. Iakoubovskii, A. Stesmans, K. Suzuki, J. Kuwabara, and A. Sawabe, Diamond Relat. Mater. **12**, 511 (2003).
[24] K. Iakoubovskii and A. Stesmans, Phys. Rev. B **66**, 195207 (2002).
[25] K. Iakoubovskii, A. Stesmans, M. Nesladek, and G. Knuyt, Phys. Status Solidi A **193**, 448 (2002).
[26] S. D. Williams, D. J. Twitchen, P. M. Martineau, G. A. Scarsbrook, and I. Friel, UK Patent Application No. GB 2428690 A (pending).
[27] D. J. Twitchen, M. E. Newton, J. M. Baker, O. D. Tucker, T. R. Anthony, and W. F. Banholzer, Phys. Rev. B **54**, 6988 (1996).
[28] D. F. Howarth, J. A. Weil, and Z. Zimpel, J. Magn. Reson. **161**, 215 (2003).
[29] J. S. Hyde, M. Pasenkiewicz-Gierula, A. Jesmanowicz, and W. E. Antholine, Appl. Magn. Reson. **1**, 483 (1990).
[30] S. C. Lawson, D. Fisher, D. C. Hunt, and M. E. Newton, J. Phys.: Condens. Matter **10**, 6171 (1998).
[31] R. M. Chrenko, H. M. Strong, and R. E. Tuft, Philos. Mag. **23**, 313 (1971).
[32] G. Davies, Physica B (Amsterdam) **273-274**, 15 (1999).
[33] G. Davies, Rep. Prog. Phys. **44**, 787 (1981).
[34] K. Iakoubovskii, G. J. Adriaenssens, N. N. Dogadkin, and A. A. Shiryaev, Diamond Relat. Mater. **10**, 18 (2001).
[35] W. V. Smith, P. P. Sorokin, I. L. Gelles, and G. J. Lasher, Phys. Rev. **115**, 1546 (1959).
[36] D. J. Twitchen, M. E. Newton, J. M. Baker, T. R. Anthony, and W. F. Banholzer, Phys. Rev. B **59**, 12900 (1999).
[37] J. R. Morton and K. F. Preston, J. Magn. Reson. **30**, 577 (1978).
[38] D. R. Lide, *CRC Handbook of Chemistry and Physics*, 87th ed. (CRC, Boca Raton, FL, 2006).
[39] A. Abragam, J. Horowitz, M. H. L. Pryce, and K. W. Morton, Proc. R. Soc. London, Ser. A **230**, 169 (1955).
[40] J. H. Wood and G. W. Pratt, Phys. Rev. **107**, 995 (1957).
[41] M. Gerloch, *Orbitals, Terms and States* (Wiley, Chichester, 1986).
[42] S. Felton, A. M. Edmonds, M. E. Newton, P. M. Martineau, D. Fisher, and D. J. Twitchen, Phys. Rev. B **77**, 081201(R) (2008).